Applied Physics A (2022) 128:1
https://doi.org/10.1007/s00339-021-05118-z

Applied Physics A
Materials Science & Processing

Microstructures and properties of $Cr_xFeNi_{(3-x)}Al$ high-entropy alloys

Wen Zhang[2] · Xicong Ye[1,2] · Dong Xu[2] · Chang Liu[2] · Dong Fang[1,2] · Bo Li[1,2]

Received: 17 May 2021 / Accepted: 19 November 2021 / Published online: 3 December 2021

Abstract
A set of novel Co-free high-entropy alloys $Cr_xFeNi_{(3-x)}Al$ (x = 0.25, 0.5, 0.75, 1, 1.25, 1.5) were fabricated by non-self-consumable vacuum melting method, and their solidification microstructures as well as compression properties were investigated. The research results firstly demonstrate that the solidification microstructures of Cr-0.25, Cr-0.5 and Cr-0.75 are composed of primary B2 phase and (FCC + B2) eutectic structure; Secondly, there are primary B2 phase and (FCC + B2) eutectic structure in the solidification microstructure of Cr-1, with a tiny amount of BCC phase distributing on the matrix of primary phase B2; In addition, as a "sunflower-like" structure of BCC phase and B2 phase, the solidification microstructure of Cr-1.25 is identified. Also, the core of the sunflower is B2 phase, and the petals are alternately arranged by BCC phase and B2 phase; Last but not least, it is a fine BCC phase and B2 dual-phase structure that form the solidification microstructure of Cr-1.5. Among the phases mentioned above, the FCC phase is abundant in Ni and Fe elements, the B2 phase is abundant in Ni and Al elements, and the BCC phase is abundant in Cr element. With the ascending trend of Cr content, the strength of $Cr_xFeNi_{(3-x)}Al$ high-entropy alloy descends initially and then climbs, during which the primary reasons for the rise of strength are solid solution strengthening, fine crystal strengthening and precipitation of BCC phase. The compressive strengths of Cr-1.25 and Cr-1.5 alloys are 2111.5 and 1985.3 MPa, respectively, and the compressibility can attain to 41.36 and 49.87%, respectively, manifesting comprehensive mechanical properties.

Keywords High-entropy alloy · Solidification microstructures · Compressive properties · Co-free

1 Introduction

Different from the first generation of high-entropy alloys(HEAs) defined by five or more equimolar ratio or nearly equimolar ratio content elements, the second generation of HEAs consists of four or more alloying elements, the content ratios of constituent elements can be non-equal atomic ratios, and the microstructure is a complex solid solution alloy with biphasic or multiphase. The emergence of this new genre opens a broader space for the design of HEAs [1–5]. Due to the high-entropy effect, sluggish diffusion, severe lattice distortion and cocktail effect [1–6], HEAs have many excellent properties, such as excellent wear resistance [7], high temperature strength and thermal stability [8, 9], high elongation [10, 11], and fatigue and fracture properties [12–14]. However, the poor fluidity, compositional segregation, and matching problems between strength and plasticity of HEAs have hindered their industrial application [15, 16].

The good fluidity of eutectic alloys makes them less likely to form dendritic segregation during solidification, and the lower melting point of eutectic alloys makes melting less difficult; thus, eutectic alloys have good casting properties [17]. Based on the above design ideas, Yiping Lu et al. [15] proposed the concept of eutectic high-entropy alloys (EHEAs) and designed AlCoCrFeNi EHEAs in 2014. Due to the advantages of both eutectic and HEAs, EHEAs have received more and more attention [18], such as $Fe_{20}Co_{20}Ni_{41}Al_{19}$ [19], $CoCrFeNiZr_{0.5}$ [20], and $Ni_{30}Co_{30}Cr_{10}Fe_{10}Al_{18}W_2$ [21].

Al-Co-Cr-Fe–Ni EHEAs have good comprehensive mechanical properties. Therefore, on the basis of $AlCoCrFeNi_{2.1}$, researchers prepared $AlCo_xCrFeNi_{3-x}$ [22], $AlCoCrFeNi_3$ [23], $Al_{17}Co_{14.3}Cr_{14.3}Fe_{28.6}Ni_{25.8}$ [23],

✉ Xicong Ye
yexc@ctgu.edu.cn

✉ Dong Fang
hill988@163.com

[1] Yichang Key Laboratory of Graphite Additive Manufacturing, China Three Gorges University, Yichang 443002, China

[2] College of Mechanical and Power Engineering, China Three Gorges University, Yichang 443002, China

$Al_{16}Co_{41}Cr_{15}Fe_{10}Ni_{18}$ [24], etc. Since the above mentioned EHEAs contain expensive Co elements, which adversely affect their industrial applications, researchers have conducted Co-free studies based on this alloy system. For example, the Co-free $CrFeNi_{(3-x)}Al_x$ EHEAs system designed by Jin et al. [25], and by studying it, it was found that the increase in Al elements promotes BCC phase formation and Ni elements are FCC phase stabilizer [26]. Dong et al. [27] designed the excellent performance $AlCrFe_2Ni_2$ HEAs based on $AlCoCrFeNi_{2.1}$ by replacing the expensive Co with equimolar cheap Fe and reducing the Ni element with a tensile yield strength of 796 MPa, ultimate strength of 1437 MPa and elongation of 15.7%. Chuan et al. [28] found that Cr element can stabilize the BCC phase in the Al-Co-Cr-Fe–Ni alloy system. Therefore, the content of BCC and FCC phases can be adjusted by adjusting the content of Cr and Ni elements to design a HEAs of AlCrFeNi system with good comprehensive mechanical properties. In this paper, a $Cr_xFeNi_{(3-x)}Al$ (x = 0.25, 0.5, 0.75, 1, 1.25, 1.5) HEAs alloy was designed to study the solidification microstructures and properties of $Cr_xFeNi_{(3-x)}Al$ HEAs by adjusting the content of Cr and Ni elements, a Co-free HEAs with good comprehensive mechanical properties.

2 Experimental

The non-equiatomic $Cr_xFeNi_{(3-x)}Al$ (x = 0.25,0.5,0.75,1,1.25,1.5) alloy ingots were synthesized by non-consumable vacuum melting the raw materials of Fe, Ni, Cr, Mn, and Al (> 99.9% pure) in a water-cooled copper crucible in pure Ar atmosphere. Each of the 30 g ingots was flipped and re-melted at least six times to improve the chemical homogeneity.

Crystal structures were identified with Ultima IV diffractometer at 40 kV/40 mA using Cu Kα radiation and scanning rate of 4°/min from 20° to 100°. The microstructures and chemical composition were examined using a Phenom Pro scanning electron microscope (SEM) coupled with a backscattered electron (BSE) and an energy-dispersive spectrometer (EDS). Samples for SEM characterization were abraded and then polish successively with diamond and silica colloidal suspension. Room-temperature compression tests under a strain rate of $5 \times 10\text{-}4\ s^{-1}$ were carried out using the WDW-100E universal tester.

3 Results and discussion

3.1 Microstructure

Figure 1a shows the X-ray diffraction patterns of the cast $Cr_xFeNi_{(3-x)}Al$ (x = 0.25, 0.5, 0.75, 1, 1.25, 1.5) HEAs. It can be seen that the $Cr_xFeNi_{(3-x)}Al$ HEAs all contain B2 phase, and with the increase in Cr content, the solidification microstructure changes from FCC + B2 phase to FCC + B2 + BCC and finally to B2 + BCC. Among them, Cr-0.25, Cr-0.5 and Cr-0.75 are FCC + B2 phase, Cr-1 microstructure is FCC + BCC + B2 phase, Cr-1.25 and Cr-1.5 alloys are consisted of BCC + B2, and FCC phase disappears or its content is below the detectable limit by XRD. When the Cr content was increased to 1, BCC diffraction peaks appeared in the tissue, and the lattice constants of the BCC and B2 phases were very close to each other, making the diffraction peaks

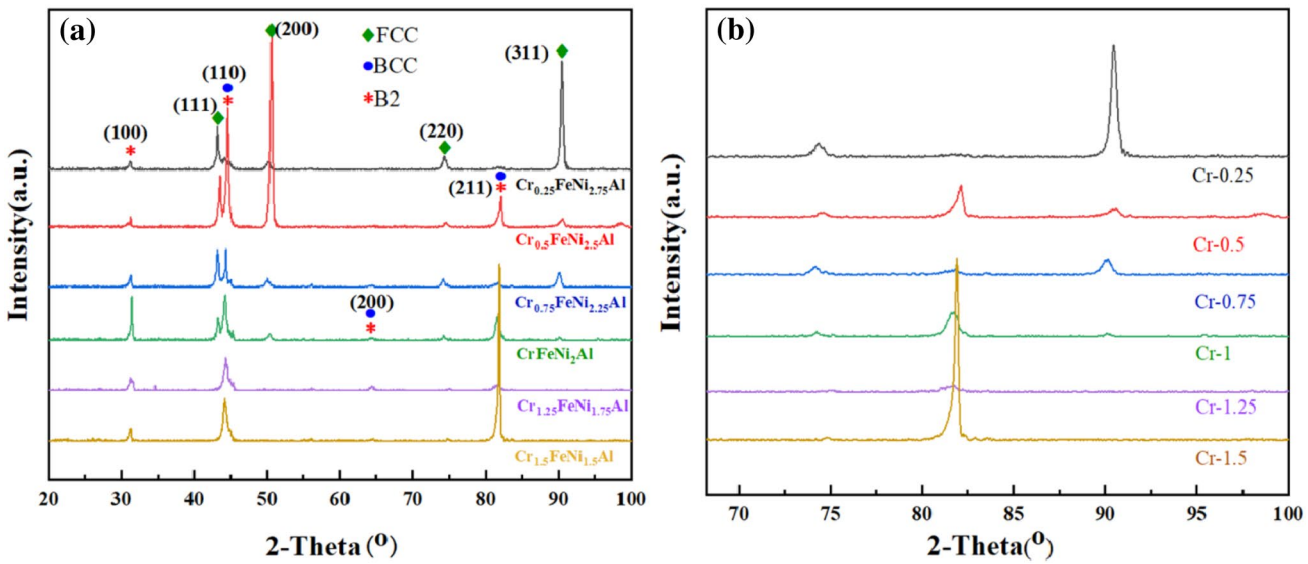

Fig. 1 XRD patterns of the $Cr_xFeNi_{(3-x)}Al$ (x = 0.25,0.5,0.75,1,1.25,1.5) HEAs. **a** as-cast; **b** Partially enlarged

of (110), (200) and (211) in the XRD spectrum overlap. Dong [27] et al. found that $AlCrFe_2Ni_2$ is FCC + BCC + B2 triple phase and the XRD pattern contains three overlapping diffraction peaks of (110), (200) and (211), Jin et al. [25] concluded that the primary phase of $CrFeNi_2Al$ is composed of B2 phase and (FCC + B2) eutectic structures, and the primary phase B2 was found to contain a large number of precipitated particles of BCC, which is consistent with the results of Cr-1 in this paper. Singh et al. [29] analyzed the phenomenon of overlapping XRD diffraction peaks of HEAs phases and concluded that the occurrence of this phenomenon is mainly due to the spinodal decomposition between the alloy components. Under the effect of spinodal decomposition, the solid solution atoms of the supersaturated solid solution become solutes of each other, and their concentration amplitudes keep increasing, while decomposing into two phases with the same structure but different compositions, which, together with similar atomic sizes, the same crystal structure and similar lattice constants. Since Cr is the stabilizer of BCC and Ni is the stabilizer of FCC [28], the decrease in Ni content with the increase in Cr content leads to the decrease in FCC phase until it disappears and the increase in BCC phase.

Figure 1b shows the XRD local magnification of the as-cast $Cr_xFeNi_{(3-x)}Al$ HEAs, and the selected region is $2\theta \approx 70° \rightarrow 100°$, because the higher the grain surface index the smaller the grain surface spacing and the more pronounced the movement of the peaks, which is easier to observe [30]. Table 1 shows the lattice constants of various phases at different Cr contents, and Table 2 shows the EDS measurements of the nominal composition and the actual composition after preparation at different Cr contents. According to the EDS results in Table 2, it can be seen that the Cr element solidly dissolved into FCC gradually increases, and the characteristic peak in Fig. 1 gradually moves to the low-angle direction as the Cr content increases, which reflects the atomic size effect of the larger radius of Cr atoms comparing Ni atoms, resulting in lattice volume expansion as well as lattice distortion, thus increasing the FCC lattice constant. The elemental content of Ni and Al in B2 does not change much, so the lattice constant of B2 phase does not change much, while the lattice constant of BCC appears to increase first and then decrease.

Figure 2 shows the SEM image of the as-cast $Cr_xFeNi_{(3-x)}Al$ HEAs. As shown in Fig. 2a–f, the Cr-0.25, Cr-0.5 and Cr-0.75 alloys consist of the incipient phase B2 and (FCC + B2) eutectic structures. According to the EDS results in Table 2 B2 is rich in Ni and Al elements, and FCC phase is rich in Ni and Fe elements, so it can be judged that the primary phase is B2 phase and the lamellae microstructure is (FCC + B2) eutectic. For the Cr-1 alloy, the incipient phase is B2 phase, and the finer lamellar microstructure is (FCC + B2) eutectic. Since some regions in Cr-1 are rich in Cr element, it can be judged that the region is BCC phase, which is consistent with the above XRD analysis results, as shown in Fig. 2(g-h). Due to the finer BCC phase, it diffusely

Table 1 The lattice constants of FCC, BCC, and B2 phases in $Cr_xFeNi_{(3-x)}Al$ (x = 0.25, 0.5, 0.75, 1, 1.25, 1.5) HEAs

HEAs	Lattice constant(Å)		
	FCC	BCC	B2
Cr-0.25	3.5403	–	2.8869
Cr-0.5	3.5405	–	2.8871
Cr-0.75	3.5853	–	2.8873
Cr-1	3.5909	2.8963	2.8876
Cr-1.25	–	2.9154	2.8878
Cr-1.5	–	2.8872	2.8880

Table 2 Nominal composition of $Cr_xFeNi_{(3-x)}Al$ HEAs and chemical analysis of different regions or phases by EDS (at%)

HEAs	Nominal component/at%	Phase	Unit: at%			
			Cr	Fe	Ni	Al
Cr-0.25	$Cr_5Fe_{20}Ni_{55}Al_{20}$	FCC	6.85	23.33	56.92	12.90
		B2	3.39	15.26	58.09	23.26
Cr-0.5	$Cr_{10}Fe_{20}Ni_{50}Al_{20}$	FCC	14.55	25.57	48.72	11.17
		B2	6.82	15.64	53.44	24.10
Cr-0.75	$Cr_{15}Fe_{20}Ni_{45}Al_{20}$	FCC	20.72	25.71	42.14	11.43
		B2	11.65	16.16	48.84	23.35
Cr-1	$Cr_{20}Fe_{20}Ni_{40}Al_{20}$	FCC	18.47	19.23	44.45	17.85
		BCC	24.20	27.09	38.25	10.46
		B2	13.44	16.04	46.33	24.19
Cr-1.25	$Cr_{25}Fe_{20}Ni_{35}Al_{20}$	BCC	42.28	29.90	21.24	6.59
		B2	11.35	13.73	50.45	24.47
Cr-1.5	$Cr_{30}Fe_{20}Ni_{30}Al_{20}$	BCC	49.73	28.87	14.42	6.97
		B2	14.42	13.83	45.01	26.74

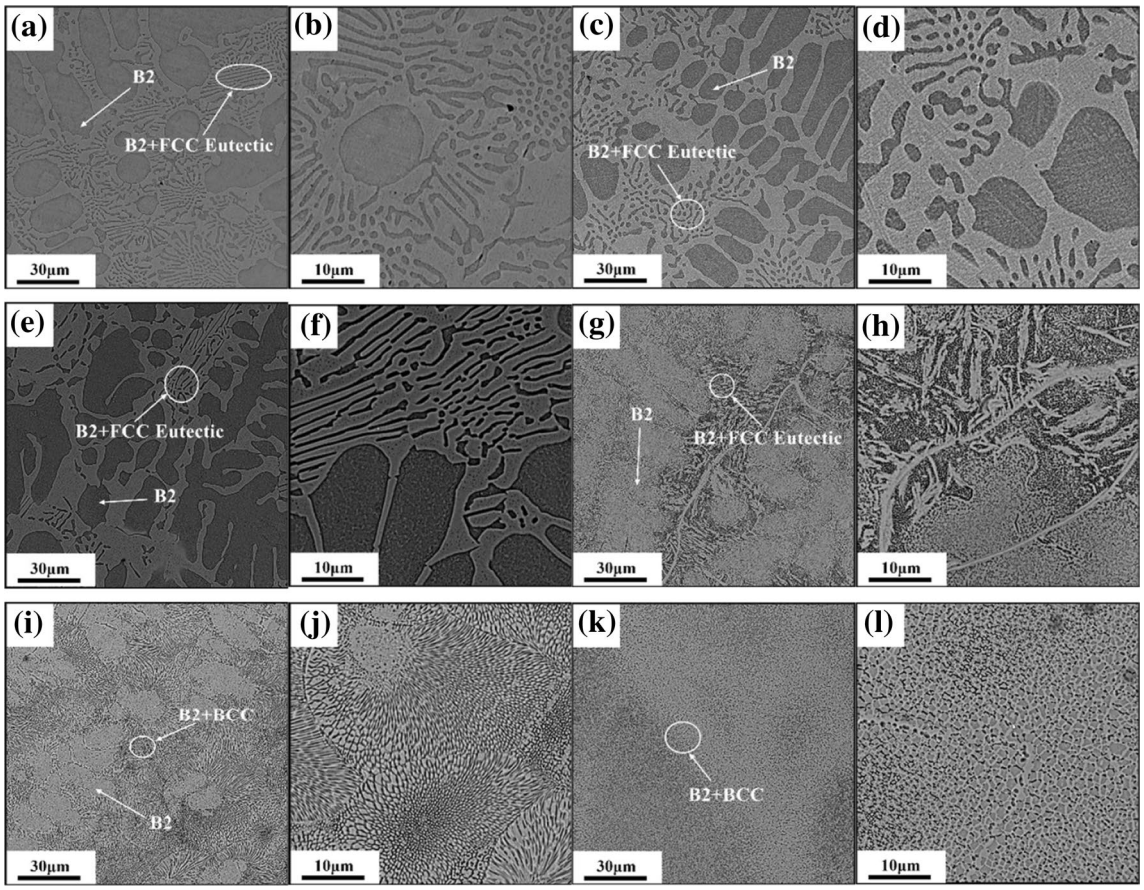

Fig. 2 SEM micrographs of as-cast $Cr_xFeNi_{(3-x)}Al$ HEAs: **a**-**b** Cr-0.25; **c**-**d** Cr-0.5; **e**-**f** Cr-0.75; **g**-**h** Cr-1; **i**-**j** Cr-1.25; **k**-**l** Cr-1.5

precipitates within the B2 phase, which is also consistent with the results of Jin et al. [25].

The continued increase in Cr content causes the microscopic morphology of the alloy to evolve from a eutectic structure to a "sunflower-like" morphology, as shown in Fig. 2i–j, divided into "core" and "petal" regions. From Fig. 2i, it can be seen that the "core" (primary phase) is the B2 phase rich in Ni and Al elements, and the "petals" (at the boundary of the primary phase) are the alternating distribution of the B2 phase rich in Ni and Al and the BCC phase rich in Cr element. The solidification microstructure of Cr-1.5 is a fine and uniform B2 + BCC phases, as shown in Fig. 2k–l. To observe the distribution of elements more clearly, the microstructure was characterized by EDS surface scanning, as shown in Fig. 3. The Cr-0.25, Cr-0.5, and Cr-0.75 microstructures clearly show that the Al and Ni elements are enriched at the incipient phase and eutectic structure, and the Ni and Fe elements are enriched in the eutectic structures region. The EDS results of Cr-1 show that Ni and Al elements are enriched in the primary phase region, Ni and Fe elements are distributed in the eutectic structure region, and Cr element is scattered within the primary phase. In Cr-1.25, Ni and Al are enriched in the primary phase, while Cr element is concentrated at the primary phase boundary. In Cr-1.5, Ni, Al and Cr elements are alternately distributed.

3.2 Mechanical properties

Figure 4 shows the compressive true stress–strain curves for the cast $Cr_xFeNi_{(3-x)}Al$ (x = 0.25, 0.5, 0.75, 1, 1.25, 1.5) HEAs at room temperature. The yield strength $\sigma_{0.2}$, ultimate compression strength σ_p, and fracture strain ε_p obtained from the curves are shown in Table 3. In general, the FCC phase contributes to the ductility of the alloy [18]; therefore, Cr-0.25, Cr-0.5 and Cr-0.75 have higher compressibility. The B2 and BCC phases contribute to the strength of the alloy [18], so Cr-1, Cr-1.25 and Cr-1.5 have higher yield and compressive strengths. The yield strength of Cr-1.25 is 1716.6 MPa, the compression strength is 2111.51 MPa, and the fracture strain is 41.36%, the yield strength of Cr-1.5 is 1650 MPa, the compression strength is 1985.25 MPa, and the fracture strain is 49.87%, which shows good comprehensive mechanical properties. The change of mechanical properties of $Cr_xFeNi_{(3-x)}Al$ high-entropy alloy is mainly attributed to: on the one hand, the change of Cr and Ni content leads to the change of

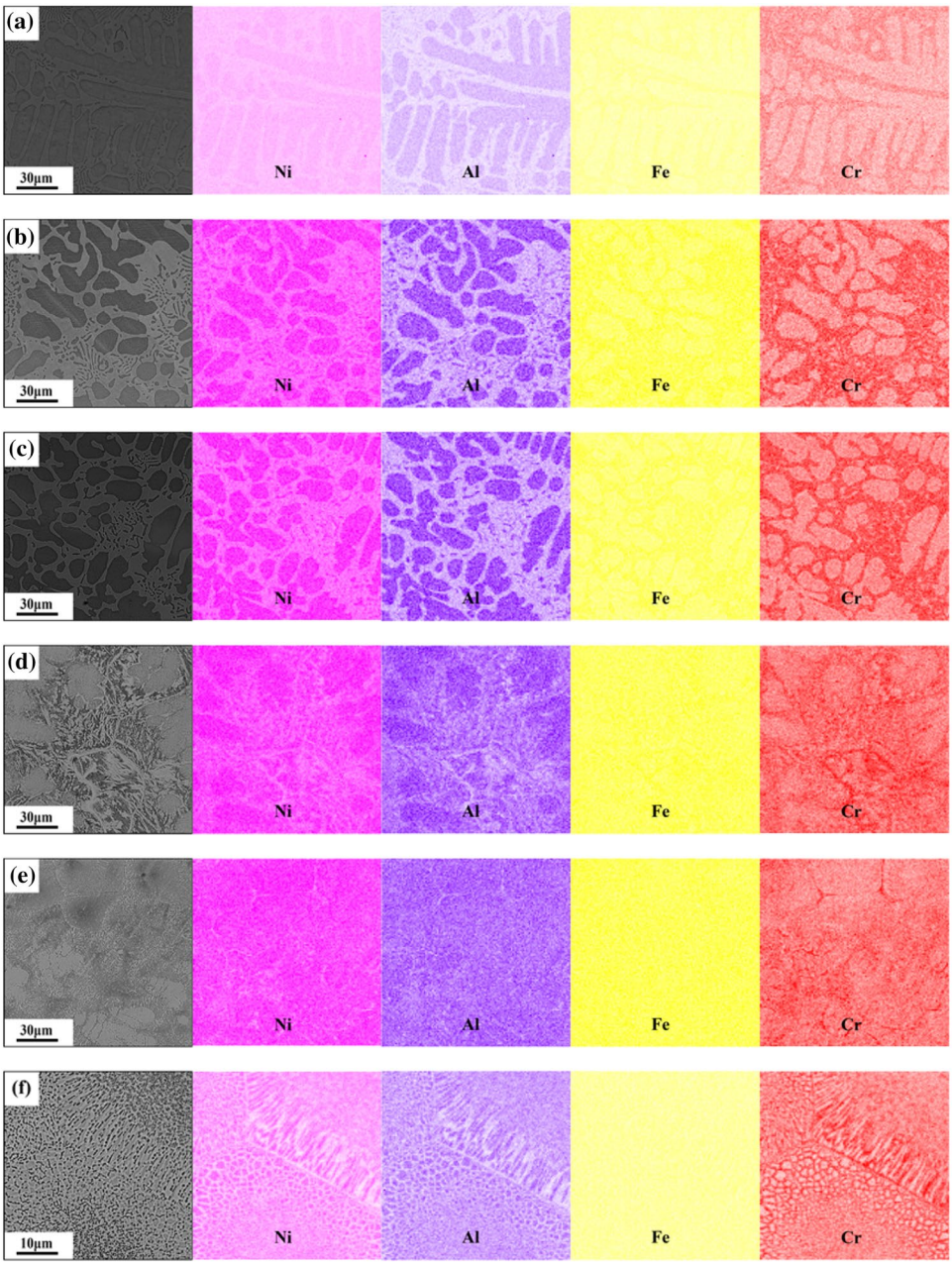

Fig. 3 EDS surface scanning micrographs of as-cast $Cr_xFeNi_{(3-x)}Al$ HEAs: **a** Cr-0.25; **b** Cr-0.5; **c** Cr-0.75; **d** Cr-1; **e** Cr-1.25; **f** Cr-1.5

microstructure of the alloy, comparing the solidification microstructure of Cr-0.75 with that of Cr-0.25 and Cr-0.5, it can be seen that the primary phase (B2) of Cr-0.75 is coarser and only a small amount of lamellar FCC + B2 eutectic structure. This makes the yield strength of Cr-0.75 significantly lower than that of Cr-0.25 and Cr-0.5. In addition, when the addition of Cr reaches 20 at% (Cr-1), part of the FCC phase in the alloy is transformed into BCC phase, so that the microstructure of the alloy changes from the primary phase B2 and eutectic FCC + B2 to FCC and BCC + B2 structure, and when the addition of Cr increases further, the microstructure of the alloy changes to B2 and B2 + BCC, and when the addition of Cr reaches 30 at% (Cr-1.5), the structure of the alloy becomes fine B2 + BCC. The B2 and BCC phases help to improve the strength of the alloy, and the Cr-1.25 and Cr-1.5 grains are finer than those of the other four compositions, which have the effect of fine grain strengthening, so they have good overall mechanical properties. On the other hand, since the atomic radius of Cr element is larger than that of Ni, with the increase in Cr element addition, more and more Cr atoms solid solution into the alloy causes lattice distortion and plays the effect of solid solution strengthening. Combined with the EDS results, the Cr element content in Cr-1.25 and Cr-1.5 is significantly higher than other alloys, so the strength is significantly improved.

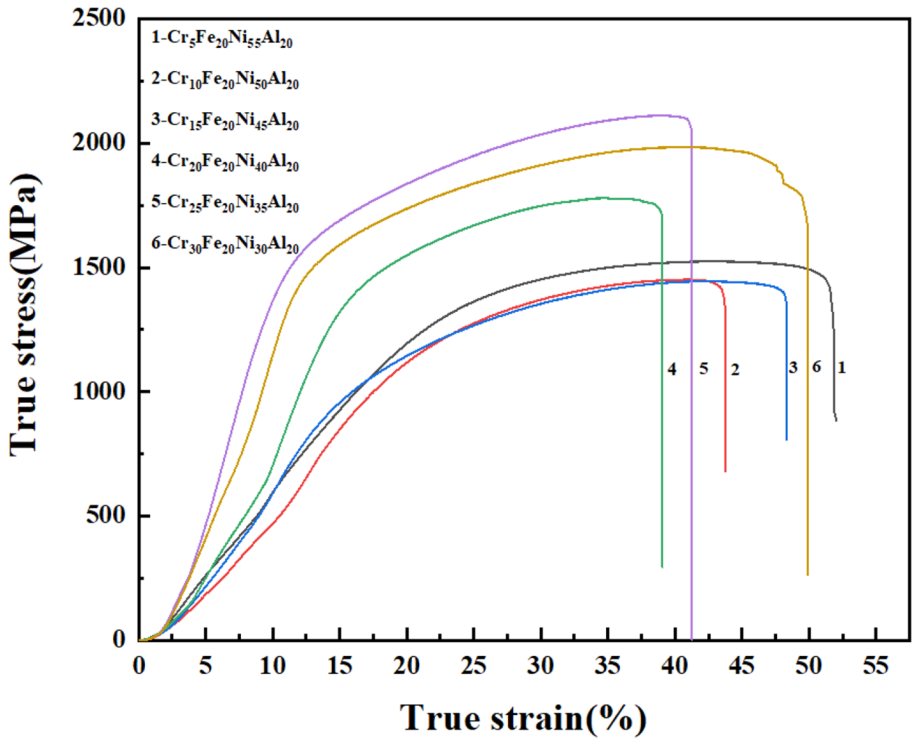

Fig. 4 Compression true stress–strain curves of the as-cast $Cr_xFeNi_{(3-x)}Al$ HEAs at room temperature

Table 3 Compression property of the as-cast $Cr_xFeNi_{(3-x)}Al$ HEAs at room temperature

HEAs	$\sigma_{0.2}$(MPa)	σ_p(MPa)	ε_p(%)	Phase
Cr-0.25	1111.3	1524.9	51.69	FCC + B2
Cr-0.5	1112.9	1451.5	43.78	FCC + B2
Cr-0.75	831.6	1444.7	48.31	FCC + B2
Cr-1	1430.9	1779.6	39.04	FCC + BCC + B2
Cr-1.25	1716.6	2111.5	41.36	BCC + B2
Cr-1.5	1650.0	1985.3	49.87	BCC + B2

Figure 5 shows a comparison of the compressibility and compressive strength of some HEAs [31–34] prepared by solidification with $Cr_xFeNi_{(3-x)}Al$ HEAs. Although the compressive strength of $Cr_xFeNi_{(3-x)}Al$ is lower than that of $AlCoCrFeNiV_x$ (x = 0.5, 0.8, 1.0) and $Al_{1.12}CoCrFeNi$, it exhibits excellent compressibility, the compressibility difference between CoCrFeNi and $Cr_xFeNi_{(3-x)}Al$ is not significant, but $Cr_xFeNi_{(3-x)}Al$ exhibits excellent compression strength, $Al_{1.12}CoCrFeNi$ and AlCrFeCoNiCu have excellent overall mechanical properties, but both contain expensive Co. It can be seen that $Cr_xFeNi_{(3-x)}Al$ has good comprehensive mechanical properties and is promising for industrial applications.

3.3 Phase prediction

Some scholars have now summarized the existing phase formation models for HEAs [35], such as Zhang Yong [36] and others who first extended the Hume-Rothery rule [37] from binary alloys to HEAs and investigated the relationship between δ (atomic radius difference) and ΔH_{mix} (mixing enthalpy). Yiping Lu [38] proposed to determine the eutectic composition in HEAs by calculating the mixing enthalpy. Guo et al. [26] defined an additional parameter VEC (valence electron concentration) to predict the phase formation pattern. Considering the competing entropy-enthalpy relationship, Yang et al. [39] scholars proposed the parameter Ω.

To investigate the phase stability of the cast $Cr_xFeNi_{(3-x)}Al$ (x = 0.25, 0.5, 0.75, 1, 1.25, 1.5) HEAs, the relevant thermodynamic parameters are calculated in this paper, and the expressions are as follows:

$$\delta = \sqrt{\sum_{i=1}^{n} c_i(1 - r_i/\bar{r})^2}, \bar{r} = \sum_{i=1}^{n} c_i r_i \tag{1}$$

$$\Delta H_{\text{mix}} = \sum_{i=1,\, i\neq j}^{n} \Delta H_{ij}^{mix} c_i c_j \tag{2}$$

$$\Omega = T_m \Delta S_{\text{mix}} / \left|\Delta H_{\text{mix}}\right|, T_m = \sum_{i=1}^{n} c_i (T_m)_i \tag{3}$$

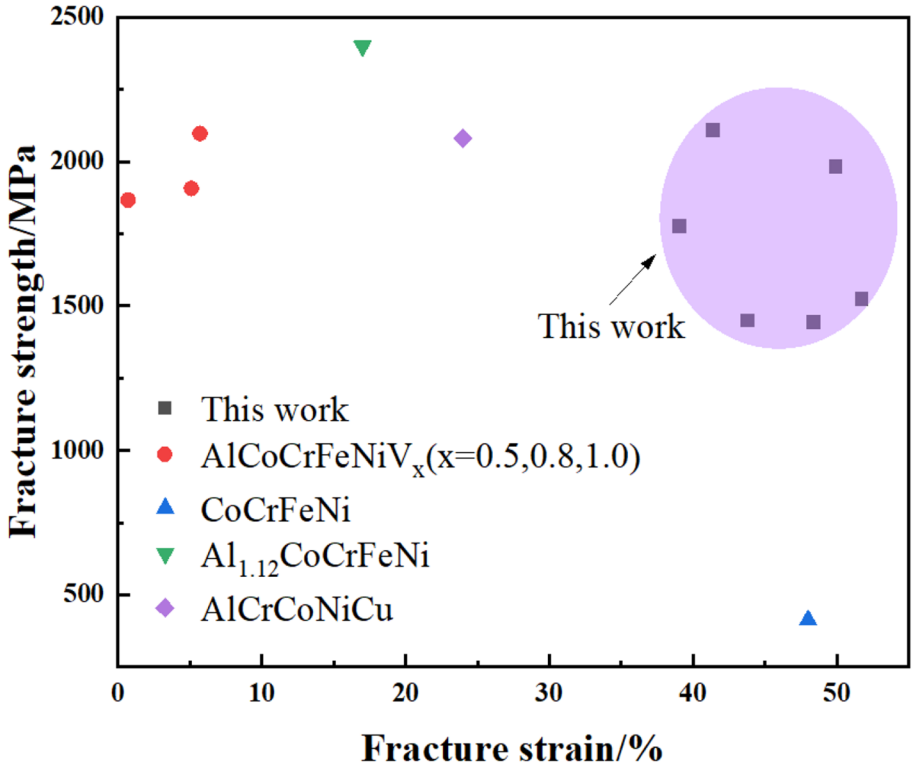

Fig. 5 Some high-entropy alloys prepared by casting method and $Cr_xFeNi_{(3-x)}Al$ HEAs compressibility-compression strength comparison graph

where i is the number of elements, $\bar{r}$ is the average atomic radius, r_i, c_i and $(T_m)_i$ are the atomic radius, atomic percentage, and melting point of the i element. Table 4 gives the relevant parameters of the $Cr_xFeNi_{(3-x)}Al$ HEAs calculated according to the above expression. Based on the description of the B2 phase in the available literature, the phase prediction is therefore discussed in this paper from two aspects: 1) The B2 phase is an ordered BCC structure [40]: According to existing literature, if $\Omega \geq 1.1$, $\delta \leq 6\%$,-15 kJ/mol $< \Delta H_{mix} <$ 5 kJ/mol then the stable solid solution forms[39]. The experimental results all satisfy the range of forming stable solid solution. The valence electron concentration proposed by Guo [26] et al. can be used to predict the formation of FCC and BCC phases in HEAs, with a tendency to form FCC solid solution when VEC $\geq$ 8 and BCC solid solution when VEC $\leq$ 6.87, and a tendency to co-exist FCC + BCC phases when the VEC is between the two [26]. The experimental results show the coexistence of FCC + B2 phase at Cr-0.25, which is not consistent with the above criterion. 2) B2 phase is a NiAl intermetallic compound [31]: the VEC criterion cannot exclude the formation of intermetallic compounds and is valid only when the alloy product is a solid solution [35]. Therefore, Yang [39] et al. attempted to separate the SS (solid solution) phase and IM (intermetallic compound) phase with Ω parameters and derived the range of IM and SS mixed phases as:$1.1 \leq \Omega \leq 10, 3.6\% \leq \delta \leq 6.6\%$. The experimental results satisfy the criterion of this IM and SS mixed phase. Therefore, the $\Omega \geq 1.1$, $\delta \leq 6.6\%$,-15 kJ/mol $< \Delta H_{mix} <$ 5 kJ/mol criterion is appropriate when B2 is considered to be an ordered BCC structure, and when B2 is considered to be a NiAl intermetallic compound, it is appropriate to use the $1.1 \leq \Omega \leq 10, 3.6\% \leq \delta \leq 6.6\%$ criterion.

Table 4 The calculated phase formation values for the $Cr_xFeNi_{(3-x)}Al$ HEAs

HEAs	δ(%)	ΔH_{mix} (KJ/mol)	VEC	ΔS_{mix} (KJ/mol)	T_m/K	Ω
Cr-0.25	5.7	– 13.53	8	9.3	1604.8	1.11
Cr-0.5	5.65	– 13.64	7.8	10.1	1625	1.21
Cr-0.75	5.59	– 13.61	7.6	10.7	1645.2	1.29
Cr-1	5.53	– 13.44	7.4	11.1	1665.4	1.37
Cr-1.25	5.46	– 13.13	7.2	11.3	1685.6	1.45
Cr-1.5	5.39	– 12.68	7	11.4	1705.8	1.53

4 Conclusions

In this study, $Cr_xFeNi_{(3-x)}Al$ (x = 0.25,0.5,0.75,1,1.25,1.5) HEAs were prepared. The solidification microstructures and mechanical properties of the alloys were investigated, and the conclusions are summarized as follows:

(1) Cr-0.25, Cr-0.5, Cr-0.75 and Cr-1 all contain eutectic structure (FCC + B2), and the primary phase is B2 phase, and Cr-1 also contains BCC phase dispersed in the B2 primary phase; Cr-1.25 contains a "sunflower-like " microstructure with B2 + BCC as "petals" and B2 phase as the "core"; Cr-1.5 has a uniform fine microstructure with B2 + BCC alternately distributed.

(2) With the increase in Cr content, the yield strength and compression strength decrease first and then increase, Cr-1.25 and Cr-1.5 have good comprehensive mechanical properties, where the yield strength of Cr-1.25 and Cr-1.5 alloys are 1716.6 and 1650 MPa respectively, the compression strength is 2111.5 MPa and 1985.3 MPa respectively, and the fracture strain is 41.36 and 49.87%, respectively.

(3) When the B2 phase is an ordered BCC structure, the $\Omega \geq 1.1$, $\delta \leq 6.6\%$ and -15 kJ/mol $< \Delta H_{mix} < 5$ kJ/mol criterion is suitable; when B2 is a NiAl intermetallic compound, the $1.1 \leq \Omega \leq 10, 3.6\% \leq \delta \leq 6.6\%$ criterion is suitable.

Acknowledgements The research was financially supported by the National Natural Science Foundation of China (Nos. 51604161), Yichang Key Laboratory of Graphite Additive Manufacturing Program (Nos. YKLGAM202001).

References

1. J.W. Yeh, S.K. Chen, S.J. Lin et al., Nanostructured high-entropy alloys with multiple principal elements: novel alloy design concepts and outcomes. Adv. Eng. Mater. **6**(5), 299 (2004). https://doi.org/10.1002/adem.200300567
2. B. Cantor, I. Chang, P. Knight et al., Microstructural development in equiatomic multicomponent alloys. Mater. Sci. Eng.: A **375**, 213 (2004). https://doi.org/10.1016/j.msea.2003.10.257
3. Z.A. Yong, A. Ttz, T.B. Zhi et al., Microstructures and properties of high-entropy alloys. Prog. Mater Sci. **61**, 1 (2014). https://doi.org/10.1016/j.pmatsci.2013.10.001
4. A.D.B.M. Bons, A critical review of high entropy alloys and related concepts. Acta Materialia **122**, 448 (2017). https://doi.org/10.1016/j.actamat.2016.08.081
5. Z.P. Liu et al., An assessment on the future development of high-entropy alloys: Summary from a recent workshop. Intermetallics **66**, 67 (2015). https://doi.org/10.1016/j.intermet.2015.06.021
6. J.-W. Yeh, Alloy Design Strategies and Future Trends in High-Entropy Alloys. JOM **65**, 1759 (2013). https://doi.org/10.1007/s11837-013-0761-6
7. M.H. Chuang, M.H. Tsai, W.R. Wang et al., Microstructure and wear behavior of AlxCo1.5CrFeNi1.5Tiy high-entropy alloys. Acta Materialia **59**(16), 6308 (2011). https://doi.org/10.1016/j.actamat.2011.06.041
8. Y. Zou, H. Ma, R. Spolenak, Ultrastrong ductile and stable high-entropy alloys at small scales. Nat. Commun. **6**, 7748 (2015). https://doi.org/10.1038/ncomms8748
9. Y.D. Wu, Y.H. Cai, T. Wang et al., A refractory Hf25Nb25Ti25Zr25 high-entropy alloy with excellent structural stability and tensile properties. Mater. Lett. **130**, 277 (2014). https://doi.org/10.1016/j.matlet.2014.05.134
10. Y. Deng, C. Tasan, K. Pradeep et al., Design of a twinning-induced plasticity high entropy alloy. Acta Mater. **94**, 124 (2015). https://doi.org/10.1016/j.actamat.2015.04.014
11. D. Li, C. Li, T. Feng et al., High-entropy Al03CoCrFeNi alloy fibers with high tensile strength and ductility at ambient and cryogenic temperatures. Acta Materialia **123**, 285 (2017). https://doi.org/10.1016/j.actamat.2016.10.038
12. B. Gludovatz, A. Hohenwarter, D. Catoor et al., A fracture-resistant high-entropy alloy for cryogenic applications. Science **345**(6201), 1153 (2014). https://doi.org/10.1126/science.1254581
13. Z. Tang, T. Yuan, C. Tsai et al., Fatigue behavior of a wrought Al0.5CoCrCuFeNi two-phase high-entropy alloy. Acta Mater. **99**, 247 (2015). https://doi.org/10.1016/j.actamat.2015.07.004
14. M.A. Hemphill, T. Yuan, G.Y. Wang et al., Fatigue behavior of Al0.5CoCrCuFeNi high entropy alloys. Acta Materialia **60**(16), 5723 (2012). https://doi.org/10.1016/j.actamat.2012.06.046
15. Y. Lu, Y. Dong, S. Guo et al., A promising new class of high-temperature alloys: eutectic high-entropy alloys. Rep **4**, 6200 (2014). https://doi.org/10.1038/srep06200
16. I.S. Wani, T. Bhattacharjee, S. Sheikh et al., Tailoring nanostructures and mechanical properties of AlCoCrFeNi2.1 eutectic high entropy alloy using thermo-mechanical processing. Mater. Sci. Eng. A **675**, 99 (2016). https://doi.org/10.1016/j.msea.2016.08.048
17. A. Ib, A. Mw, B. Zw, Eutectic/eutectoid multi-principle component alloys: a review. Mater. Charact. **147**, 545 (2019). https://doi.org/10.1016/j.matchar.2018.07.030
18. X. Ye et al., A new infinite solid solution strategy to design eutectic high entropy alloys with B2 and BCC structure. Scripta Materialia. **199**, 74128 (2021). https://doi.org/10.1016/j.scriptamat.2021.113886.
19. J. Xi, Z. Yang, Z. Lu et al., A novel Fe20Co20Ni41Al19 eutectic high entropy alloy with excellent tensile properties-ScienceDirect. Mater. Lett. **216**, 144 (2018). https://doi.org/10.1016/j.matlet.2018.01.017
20. S. Vrtnik, S. Guo, S. Sheikh et al., Magnetism of CoCrFeNiZrx eutectic high-entropy alloys. Intermetallics **93**, 122 (2018). https://doi.org/10.1016/j.intermet.2017.11.017
21. Q. Wu, Z. Wang, T. Zheng et al., A casting eutectic high entropy alloy with superior strength-ductility combination[J]. Mater. Lett. **253**, 268 (2019). https://doi.org/10.1016/j.matlet.2019.06.067
22. Y. Dong, Z. Yao, X. Huang et al., Microstructure and mechanical properties of AlCoxCrFeNi3-x eutectic high-entropy-alloy system. J. Alloys Compounds **823**, 153886 (2020). https://doi.org/10.1016/j.jallcom.2020.153886
23. X. Jin, Y. Zhou, L. Zhang et al., A new pseudo binary strategy to design eutectic high entropy alloys using mixing enthalpy and valence electron concentration. Mater. Des. **143**, 49 (2018). https://doi.org/10.1016/j.matdes.2018.01.057
24. A. Shafiei, S. Rajabi, A cobalt-rich eutectic high-entropy alloy in the system Al–Co–Cr–Fe–Ni. Appl. Phys. A **125**, 11 (2019). https://doi.org/10.1007/s00339-019-3084-9
25. J. Xi, J. Bi, Z. Lu et al., A new CrFeNi2Al eutectic high entropy alloy system with excellent mechanical properties. J. Alloy.

Compd. **770**, 655 (2019). https://doi.org/10.1016/j.jallcom.2018.08.176
26. G. Sheng, C. Ng, L. Jian et al., Effect of valence electron concentration on stability of fcc or bcc phase in high entropy alloys. J. Appl. Phys. **109**(10), 213 (2011). https://doi.org/10.1063/1.3587228
27. X. Yong Dong, YLu. Gao et al., A multi-component AlCrFe2Ni2 alloy with excellent mechanical properties. Mater. Lett. **169**, 62 (2016). https://doi.org/10.1016/j.matlet.2016.01.096
28. C. Zhang, Z. Fan, S. Chen et al., Computational thermodynamics aided high-entropy alloy design,. JOM: J. Minerals Metals Mater. Soc. **64**(7), 839 (2012). https://doi.org/10.1007/s11837-012-0365-6
29. A. Subramaniam Anil et al., On the formation of disordered solid solutions in multi-component alloys. J. Alloys Compounds: Interdiscipl. J. Mater. Sci. Solid-state Chem. Phys. **587**, 113 (2014). https://doi.org/10.1016/j.jallcom.2013.10.133
30. Q.W. Tian, G.J. Zhang et al., Homogenization of AlxCoCrFeNi high-entropy alloys with improved corrosion resistance. Mater. Charact. **151**, 302 (2019)
31. D.B. Miracle, Overview No. 104 the physical and mechanical properties of NiAl. Acta Metallurgica Et Materialia **41**(3), 649 (1993). https://doi.org/10.1016/0956-7151(93)90001-9
32. W.H. Liu, J.Y. He, H.L. Huang et al., Effects of Nb additions on the microstructure and mechanical property of CoCrFeNi high-entropy alloys. Intermetallics **60**, 1 (2015). https://doi.org/10.1016/j.intermet.2015.01.004
33. M. Yue, B. Jiang, C. Li et al., The BCC/B2 morphologies in AlxNiCoFeCr high-entropy alloys. Metals-Open Access Metall. J. **7**(2), 57 (2017). https://doi.org/10.3390/met7020057
34. B.S. Li, Y.P. Wang, M.X. Ren et al., Effects of Mn Ti and V on the microstructure and properties of AlCrFeCoNiCu high entropy alloy. Mater Sci Eng A **498**(1–2), 482 (2008). https://doi.org/10.1016/j.msea.2008.08.025
35. Z. Xuerou, L. Yukun, S. Tuo, Advances in the study of phase formation theory of high entropy alloys. Mater. Guide **33**(7), 1174 (2019)
36. Y, Zhang, et al., Solid-solution phase formation rules for multi-component alloys. Adv. Eng. Mater. **10**(6), 534 (2008). https://doi.org/10.1002/adem.200700240
37. P. Jinsheng, Q. Jianmin, T. Minbo, *Fundamentals of materials science* (Tsinghua University Press, Beijing, 2006)
38. Y.P. Lu, H. Jiang, S. Guo et al., A new strategy to design eutectic high-entropy alloys using mixing enthalpy. Intermetallics **91**, 124 (2017). https://doi.org/10.1016/j.intermet.2017.09.001
39. X. Yang, Y. Zhang, Prediction of high-entropy stabilized solid-solution in multi-component alloys-ScienceDirect. Mater. Chem. Phys. **132**(2), 233 (2012). https://doi.org/10.1016/j.matchemphys.2011.11.021
40. Dong Yong. Fundamental study on microstructure and mechanical properties in multi-phase Al-Cr-Fe-Ni-M high entropy alloys, (2016).